Feasibility of extracting the proton weak charge from quantum-control measurements of atomic parity violation on the 2*s*−3*s* or 2*s*−4*s* transition in hydrogen

Jiguang Li (李冀光),[1,*] Andrei Derevianko,[2,†] and D. S. Elliott[3,4,5,‡]

[1]Institute of Applied Physics and Computational Mathematics, Beijing 100088, China
[2]Department of Physics, University of Nevada, Reno, Nevada 89557, USA
[3]Department of Physics and Astronomy, Purdue University, West Lafayette, Indiana 47907, USA
[4]School of Electrical and Computer Engineering, Purdue University, West Lafayette, Indiana 47907, USA
[5]Purdue Quantum Science and Engineering Institute, Purdue University, West Lafayette, Indiana 47907, USA

(Received 23 October 2023; accepted 19 December 2023; published 12 January 2024)

We explore the feasibility of extracting electroweak observables from a measurement of atomic parity violation in hydrogen. Our proposed quantum-control scheme focuses on the $2s-3s$ or $2s-4s$ transitions in hydrogen. This work is motivated by the recently observed anomaly in the W-boson mass, which may substantially modify the Standard Model value of the proton weak charge. We also study the accuracy of the previously employed approximations in computing parity-violating effects in hydrogen.

DOI: 10.1103/PhysRevA.109.012808

I. INTRODUCTION

Atomic parity violation (APV) is a powerful probe of the low-energy electroweak sector of the Standard Model (SM) of elementary particles. The APV results are both unique and complementary to those from particle colliders, in particular because APV probes Z-boson exchange at low momentum transfer Q ($Q \sim \hbar/r_p \approx 0.2\,\mathrm{GeV}/c$ for a nucleus of size $\sim r_p \sim$ fm). The already demonstrated precision of table-top APV experiments and theoretical interpretations places important constraints on exotic beyond-SM physics; these are often competitive to those derived from colliders. The rich history of APV and its implications were reviewed recently in Refs. [1,2]. We will use APV and parity nonconservation (PNC) interchangeably.

Microscopically, APV is caused by the weak interaction mediated by the exchange of a Z boson. The relevant contribution to the SM Hamiltonian density reads [3]

$$\mathcal{H}_{\mathrm{PV}} = \frac{G_{\mathrm{F}}}{\sqrt{2}} \sum_q \big[C_q^{(1)}\, \bar{e}\gamma_\mu\gamma_5 e\, \bar{q}\gamma^\mu q + C_q^{(2)}\, \bar{e}\gamma_\mu e\, \bar{q}\gamma^\mu\gamma_5 q + C_q^{(3)} \partial_\nu(\bar{e}\sigma^{\mu\nu} e)\bar{q}\gamma^\mu\gamma_5 q\big], \tag{1}$$

where the Fermi constant $G_{\mathrm{F}} \approx 2.22254 \times 10^{-14}$ a.u., the summation is over quarks, e and q are field operators for electrons and quarks, respectively, and γ's are the conventional Dirac matrices [4].

The coupling of the electron axial-vector currents to the quark vector currents is parameterized by the constants $C_q^{(1)}$; the constants $C_q^{(2)}$ describe the coupling of the electron vector currents to quark axial-vector currents. The $C_q^{(1)}$ contributions lead to nuclear-spin-independent interactions and $C_q^{(2)}$ to the nuclear-spin-dependent interactions. The $C_q^{(3)}$ contribution is due to the "anomalous weak moment" and it also leads to nuclear-spin-dependent effects.

The weak Hamiltonian (1) can be simplified further by lumping quarks into nucleons (e.g., a proton is composed of two up and one down quarks)

$$\mathcal{H}_{\mathrm{PV,p}} = \frac{G_{\mathrm{F}}}{\sqrt{2}} \big[C_p^{(1)}\, \bar{e}\gamma_\mu\gamma_5 e\, \bar{p}\gamma^\mu p + C_p^{(2)}\, \bar{e}\gamma_\mu e\, \bar{p}\gamma^\mu\gamma_5 p + C_p^{(3)} \partial_\nu(\bar{e}\sigma^{\mu\nu} e)\bar{p}\gamma^\mu\gamma_5 p\big], \tag{2}$$

where we omitted couplings to neutrons because of our interest in the hydrogen atom. In general, the couplings to protons and neutrons read [5]

$$C_p^{(1)} = 2C_u^{(1)} + C_d^{(1)} = \tfrac{1}{2}(1 - 4\sin^2\theta_{\mathrm{W}}), \tag{3a}$$

$$C_n^{(1)} = C_u^{(1)} + 2C_d^{(1)} = -\tfrac{1}{2}, \tag{3b}$$

$$C_p^{(2)} = -C_n^{(2)} = g_A C_p^{(1)}, \tag{3c}$$

reflecting the quark composition of nucleons. Here θ_{W} is the Weinberg angle and $g_A \approx 1.28$ is the scale factor accounting for the partially conserved axial vector current. Finally, the anomalous weak moment contribution is suppressed by the small value of the fine-structure constant α as $C_p^{(3)} \approx \alpha/(2\pi)C_p^{(2)}$. Notice that the more conventional parametrization of the proton spin-independent coupling $C_p^{(1)}$ is in terms of the proton weak charge $\mathcal{Q}_{\mathrm{W}}^p$. At the tree level (i.e., excluding radiative corrections)

$$\mathcal{Q}_{\mathrm{W}}^p = 2C_p^{(1)}. \tag{4}$$

Since $\sin^2\theta_{\mathrm{W}} \approx 1/4$, the neutron contribution $C_n^{(1)}$ dominates $\mathcal{H}_{\mathrm{PV}}$ in all atoms except for the hydrogen atom. As a consequence, hydrogen is uniquely sensitive to $\sin^2\theta_{\mathrm{W}}$ potentially enabling its extraction at the low momentum transfer

*li_jiguang@iapcm.ac.cn
†andrei@unr.edu
‡daniel.s.elliott.1@purdue.edu

[6,7]. This is the motivation for our focus on the hydrogen atom, as the experiments with heavy atoms, such as cesium [8] or ytterbium [9], are predominantly sensitive to the neutron coupling constant $C_n^{(1)}$. In addition, compared to heavy atoms, hydrogen offers a much cleaner theoretical interpretation, avoiding all the complexities of solving the relativistic many-body problem.

To reiterate, hydrogen APV is uniquely sensitive to $\sin^2\theta_{\rm W}$ due to the absence of the otherwise leading neutron contribution. This makes it an intriguing probe of the recently reported 7σ anomaly in the mass M_W of the W boson [10]. The 7σ anomaly translates into the W boson being heavier by 0.1%. The implications of the W-boson mass for the hydrogen APV were considered in Ref. [11]. These authors pointed out that, ignoring the radiative corrections, $\sin^2\theta_{\rm W} = 1 - M_W^2/M_Z^2$, so that the 0.1% shift in M_W is equivalent to a $\sim$0.5% reduction in the $\sin^2\theta_{\rm W}$ value. This shift in the Weinberg angle is, however, strongly amplified in the $C_p^{(1)}$ determination due to $\sin^2\theta_{\rm W} \approx 1/4$, see Eq. (3a). With the recent determination [10] of the W-boson mass taken at face value, the proton spin-independent coupling $C_p^{(1)}$ value [or, equivalently, $\mathcal{Q}_{\rm W}^p$, see Eq. (4)] shifts by a sizable 3% [11] from its previously accepted SM value.

The proton weak charge $\mathcal{Q}_{\rm W}^p$ is deduced by the $Q_{\rm weak}$ collaboration [7] from the measurements of parity-violating asymmetry in the scattering of polarized electrons on protons at the Jefferson Laboratory. Their reported value is

$$\mathcal{Q}_{\rm W}^p = 0.0719(45), \tag{5}$$

which we will use as the nominal value in the rest of the paper. The $Q_{\rm weak}$ collaboration result is in agreement with the currently recommended SM value [12]

$$\mathcal{Q}_{\rm W}^p({\rm SM}) = 0.0709(2). \tag{6}$$

Notice that the fractional uncertainty in the $Q_{\rm weak}$ collaboration result is 6% and cannot decisively resolve the 3% W-boson mass anomaly shift [11]. Determination of the proton weak charge at a $\sim$1% level would be an important step in this direction.

Now we simplify the weak interaction Hamiltonian density $\mathcal{H}_{\rm PV,p}$, Eq. (2), by taking the nonrelativistic limit for the proton motion. Then $\bar{p}\gamma^\mu p \to \psi_p^\dagger\psi_p\delta_{\mu,0}$ and $\bar{p}\gamma^\mu\gamma_5 p \to \psi_p^\dagger(\sigma_p)_i\psi_p\delta_{\mu,i}$, where ψ_p is the nonrelativistic proton wave function including spin and $\boldsymbol{\sigma}_p$ is the proton Pauli matrix. The first limiting expression gives rise to the proton spin-independent contribution, while the second to the spin-dependent terms. Recall that the nuclear density $\rho_p(\mathbf{r}) = \psi_p^\dagger\psi_p$, leading to the effective operator in the electron sector

$$H_{\rm W} = -\frac{G_{\rm F}}{\sqrt{8}}\gamma_5\mathcal{Q}_{\rm W}^p\rho_p(r). \tag{7}$$

Here the proton distribution is normalized as $\int_0^\infty 4\pi r^2\rho_p(r)dr = 1$. A similar simplification can be carried out for the proton spin-dependent contributions. We quote the limiting result for the point-like proton and nonrelativistic electron [13]

$$V_{\rm PV} = \frac{G_{\rm F}}{\sqrt{8}m_e c}\big\{ - C_p^{(1)}[\boldsymbol{\sigma}\cdot\boldsymbol{p}, \delta(\boldsymbol{r})]_+ + C_p^{(2)}[\boldsymbol{\sigma}_p\cdot\boldsymbol{p}, \delta(\boldsymbol{r})]_+ - i\big(C_p^{(2)} + C_p^{(3)}\big)[(\boldsymbol{\sigma}\times\boldsymbol{\sigma}_p)\cdot\boldsymbol{p}, \delta(\boldsymbol{r})]_-\big\}. \tag{8}$$

Here $\boldsymbol{p}$ is the electron linear momentum operator and Pauli matrices $\boldsymbol{\sigma}$ act on the electron spin. $[A, B]_+$ and $[A, B]_-$ denote anticommutators and commutators, respectively. Notice the addition of the $C_p^{(2)}$ and $C_p^{(3)}$ constants in the last contribution to the potential. Since $C_p^{(3)}/C_p^{(2)} \approx \alpha/(2\pi) \ll 1$, we will neglect the anomalous weak moment contribution in our analysis.

Previous efforts to measure parity violation in atomic hydrogen were initiated in the mid-1970s at the University of Michigan [13–17], Yale University [18–20], and the University of Washington [21–23], and continued through the early 1990s. In each of these programs, the investigators attempted to detect the microwave transition between two metastable hyperfine components of the $2s\,^2S_{1/2}$ state. This transition is nominally electric-dipole ($E1$) forbidden, but due to the weak interaction, it becomes slightly $E1$ allowed. The group at Yale worked at zero magnetic field, while the Michigan and Washington groups applied a static magnetic field of $\sim$553 Gauss to Zeeman tune components of the $2s\,^2S_{1/2}$ and $2p\,^2P_{1/2}$ states into near degeneracy to take advantage of the expected resonance-enhancement of the mixing. At this level crossing, the measurement is primarily sensitive to the coupling coefficient $C_p^{(2)}$ [13]. In each case, the investigators used an interference between the parity nonconserving interaction and a parity conserving interaction to amplify the first, as first suggested by Bouchiat and Bouchiat [24,25] in 1974–75. The Michigan group, which at its conclusion achieved a higher sensitivity than the Yale or Washington groups, reported a value of $C_p^{(2)} = 1.5 \pm 1.5_{\rm stat} \pm 22_{\rm syst}$ [17], where the first uncertainty is the statistical uncertainty, and the second is due to systematic factors. The primary source of the systematic uncertainty resulted from the rotation of the microwave cavity, the so-called ϕ reversal in their measurement scheme. Note that this systematic uncertainty is greater than the SM value for $C_p^{(2)} = 0.0430$ by a factor of $\sim$500.

Recently, several papers have appeared in which the authors considered the prospects for renewed measurements in hydrogen [26–30]. The development of techniques for (i) generating beams of hydrogen of higher density, lower mean velocity, and decreased velocity dispersion [31–37], and (ii) efficient optical excitation of the metastable $2s\,^2S_{1/2}$ state [37], could lead to significant improvements, should they be employed in a new hydrogen PNC effort.

In this work, we reconsider the possibility of an *optical* APV measurement in hydrogen based on the $2s\,^2S_{1/2} \to 3s\,^2S_{1/2}$ transition at a wavelength of 656.46 nm, or the $2s\,^2S_{1/2} \to 4s\,^2S_{1/2}$ transition at a wavelength of 486.27 nm. An APV measurement on the first was considered previously by Lewis and Williams [14], and more recently by Rasor and Yost [30]. In Sec. II, we calculate the matrix elements of weak interaction Hamiltonian between the $3s$ and $3p_{1/2}$ states and between the $4s$ and $4p_{1/2}$ states, using relativistic wave functions, and including the effect of the finite size of the nucleus. This theoretical approach is more sophisticated compared to the earlier literature, in part, to match the accuracy of the SM value of the proton weak charge, Eq. (6). In Sec. III, we use these results to determine the magnitude of the parity violating amplitude for these two transitions, identify the Zeeman crossings that could be useful in extracting the coupling coefficients $C_p^{(1)}$ and $C_p^{(2)}$, and briefly outline a possible measurement scheme based on interfering coherent interactions, using two-photon absorption as the local oscillator signal. While we do not explicitly consider deuterium in this work, similar measurements in this system offer the possibility of determining $C_n^{(1)}$ and $C_n^{(2)}$ as well, as has been recognized previously [27].

II. THEORY

In the previous section, we reviewed the theory of electroweak interactions as it relates to APV. Here we focus on evaluating weak-interaction matrix elements for hydrogen and refine the previous literature analysis by using fully relativistic treatment and a realistic nuclear distribution.

The weak interaction of Eq. (7) is a pseudoscalar operator, mixing atomic states of opposite parity and of the same total angular momenta. Explicitly, the parity-mixed states $\overline{|n\ell_j m_j\rangle}$ can be expanded over the conventional parity-proper states $|n\ell_j m_j\rangle$ as

$$\overline{|ns_{1/2}m_j\rangle} = |ns_{1/2}m_j\rangle + \sum_{n'=2}^{\infty} \eta_{nn'}|n'p_{1/2}m_j\rangle, \tag{9}$$

where the mixing coefficients $\eta_{nn'}$ can be computed perturbatively

$$\eta_{nn'} = \frac{\langle n'p_{1/2}m_j|H_{\mathrm{W}}|ns_{1/2}m_j\rangle}{E_{ns} - E_{n'p_{1/2}} + \frac{i}{2}(\Gamma_{n'p_{1/2}} - \Gamma_{ns})}. \tag{10}$$

Here Γ's are the (radiative) level widths. In hydrogen-like systems, the dominant admixtures for the excited $ns_{1/2}$ states comes from $n' = n$ due to level degeneracies. We remind the reader that for a point-like nucleus the $ns_{1/2}$ and $np_{1/2}$ levels remain degenerate even in the fully relativistic treatment; only the QED and finite nuclear size corrections lift this degeneracy. We also assume that there are no external fields applied and discard the nuclear-spin-dependent effects; these will be addressed in Sec. III.

The relevant matrix element of the weak interaction (7) reads

$$\begin{aligned}\langle np_{1/2}m_j|H_{\mathrm{W}}|ns_{1/2}m_j\rangle &= -i\frac{G_{\mathrm{F}}}{\sqrt{8}}\mathcal{Q}_{\mathrm{W}}^p \\ &\times \int_0^\infty dr\rho_p(r)[F^*_{np_{1/2}}(r)G_{ns}(r) - G^*_{np_{1/2}}(r)F_{ns}(r)],\end{aligned} \tag{11}$$

where F and G are the large and small radial components of relativistic bispinors [38]. The matrix element does not depend on the value of magnetic quantum number m_j, reflecting the pseudoscalar nature of the interaction. It is worth emphasizing that the expression is fully relativistic in electron degrees of freedom and involves proton distribution $\rho_p(r)$. The same nuclear charge distribution also affects the wave functions. Below we explore the effects of various approximations in computing weak-interaction matrix element (11). We start by using a point-like nucleus $\rho_p(r) \propto \delta(r)$ both in the computation of wave functions and while evaluating the matrix element. This leads to a fully relativistic result that recovers literature expressions in the nonrelativistic limit. Then we proceed to computations with a more realistic nuclear distribution.

With relativistic orbitals [39] for H-like ions and point-like nucleus, we obtain the matrix element

$$\begin{aligned}\langle np_{1/2}m_j|H_{\mathrm{W}}|ns_{1/2}m_j\rangle &= i\frac{\sqrt{2}}{2\pi}G_{\mathrm{F}}\mathcal{Q}_{\mathrm{W}}^p Z^4\alpha\frac{\Gamma(2\gamma+1+n_r)}{\Gamma^2(2\gamma+1)} \\ &\times \left[\frac{n-1}{n_r!N^5\sqrt{N^2-1}}\right] \\ &\times \exp\left[(Z\alpha)^2 \ln\frac{1}{\rho}\right].\end{aligned} \tag{12}$$

Here, α is the fine-structure constant, nuclear charge $Z = 1$ for hydrogen, $\gamma = \sqrt{1-(\alpha Z)^2}$, the radial quantum number $n_r = n - 1$, $N = [n^2 - 2n_r(1-\gamma)]^{1/2}$, and $\rho = 2\lambda r$ with $\lambda = Z/N$. It should be emphasized that the analytical relativistic wave functions used in arriving at Eq. (12) were obtained using the point-like nucleus. In other words, the effect of the nuclear density distribution on the wave functions has been neglected. A direct consequence of this assumption is the singularity in the $j = 1/2$ relativistic wave functions, leading to the appearance of the factor $\exp[(Z\alpha)^2 \ln\frac{1}{\rho}] \propto r^{-(\alpha Z)^2}$ in Eq. (12). For hydrogen, this is a mildly diverging factor in the $r \to 0$ limit. Varying $r = 10^{-6}$ a.u. to $r = 10^{-5}$ a.u. ($\approx$2 fm) modifies this factor by just $\sim$0.01% for $Z = 1$. A natural scale for r is the proton charge radius, $r_p = 0.84\,\mathrm{fm} \approx 1.59 \times 10^{-5}$ a.u.. Moreover, the divergence is easily cured using a more realistic nuclear charge distribution while evaluating the integral in Eq. (7), see below. Also the divergence goes away if the wave functions are computed using realistic nuclear charge distributions, see, e.g., Ref. [40].

The nonrelativistic limit of the PNC matrix element of Eq. (12) reads

$$\langle np_{1/2}m_j|H_{\mathrm{W}}|ns_{1/2}m_j\rangle \approx i\frac{\sqrt{2}}{8\pi}G_F\mathcal{Q}_{\mathrm{W}}^p Z^4\alpha\left[\frac{\sqrt{n^2-1}}{n^4}\right], \tag{13}$$

where we took the $\alpha Z \to 0$ limit, so that $\gamma \approx 1$, $N \approx n$, and $\exp[(\alpha Z)^2 \ln\frac{1}{\rho}] \approx 1$. This limiting expression recovers the literature results [13,41,42]. This expression implies the $1/n^3$ scaling for PNC matrix elements.

We calculated PNC matrix elements for the $2s_{1/2} - 2p_{1/2}$, $3s_{1/2} - 3p_{1/2}$, and $4s_{1/2} - 4p_{1/2}$ pairs of states in different approximations and collected these results in Table I. The nonrelativistic (NR) PNC matrix elements in the point-like nucleus (PN) approximation, labeled as PN-NR, were obtained with Eq. (13) and their relativistic counterparts PN-R, with Eq. (12), where we used $r = 10^{-6}$ a.u. At the next step we explore the effect of using the finite-sized nucleus (FN) instead of the point-like nucleus. The nuclear distribution $\rho_p(r)$ can modify the PNC matrix elements in two distinct ways: (i) $\rho_p(r)$ appears directly in the integral (11) and (ii) it can

TABLE I. Weak interaction matrix elements $-i\langle np_{1/2}m_j|H_{\rm W}|ns_{1/2}m_j\rangle$ (in a.u.) multiplied by 10^{21}. PN: point-like nuclear distribution in the PNC Hamiltonian; FN: Fermi nuclear charge distribution in the PNC Hamiltonian; NR: nonrelativistic wave functions obtained with the point-like nuclear potential; R: relativistic wave functions obtained with the point-like nuclear potential. The column marked "Full" includes full numerical relativistic treatment where we used Fermi distribution in computing both the wave functions and the PNC matrix element (11).

	PN-NR	FN-NR	PN-R	FN-R	Full
$2s-2p_{1/2}$	71.03	71.03	71.09	71.07	71.07
$3s-3p_{1/2}$	22.91	22.91	22.93	22.92	–
$4s-4p_{1/2}$	9.927	9.927	9.935	9.930	–

modify the atomic wave functions in the nuclear region. To model finite-sized nuclear distribution we employed the Fermi distribution

$$\rho_p(r) = \frac{\rho_0}{1+\exp[(r-c)/a]}, \tag{14}$$

where c is the 50% falloff radius of the charge distribution, a is related to the 90% to 10% falloff distance t as $t = 4\ln 3\, a$, and ρ_0 is the normalization constant. For the proton we used $c = 0.4$ fm and $a = 0.18$ fm to fit the proton root-mean-square radius ($r_p \sim 0.855$ fm).

FN-NR and FN-R entries in Table I show the direct effect of the proton charge distribution $\rho_p(r)$ as in these approximations we use the analytic nonrelativistic and relativistic wavefunctions for a point-like nucleus. In the FN-NR approximation, we use the Pauli approximation in Eq. (7) to arrive at the PNC operator [43]

$$H_{\rm W}^{\rm NR} = \frac{1}{2c}\frac{G_F}{\sqrt{8}}Q_W[(\boldsymbol{\sigma}\cdot\mathbf{p})^\dagger\rho_p(r) + \rho_p(r)(\boldsymbol{\sigma}\cdot\mathbf{p})], \tag{15}$$

where the dagger form of the operator $(\boldsymbol{\sigma}\cdot\mathbf{p})$ acts on the bra when computing matrix elements.

Finally, in addition to the direct effect in Eq. (11), the proton charge distribution modifies atomic wave functions, in turn, shifting the values of the PNC matrix elements. To account for this "indirect" effect, we solve the radial Dirac equation numerically with the Fermi distribution (14). As can be seen from the last column (marked Full) of Table I, the influence of the finite-size proton on the $2s-2p_{1/2}$ PNC matrix element is negligible due to the smallness of proton. This indirect effect can be ignored for the $3s-3p_{1/2}$ and $4s-4p_{1/2}$ PNC matrix elements since the atomic wave functions with larger principal quantum numbers are pushed further away from the origin.

Examining numerical results in Table I, we find that the dominant effect on the PNC matrix elements is due to using relativistic wavefunctions, rather than the finite nuclear size effect. The matrix element variations across different approximations for nuclear distributions are just ~0.02%, which is well below the current 0.3% uncertainty in the SM proton weak charge value (6). This statement must be contrasted with APV in ^{133}Cs, where the uncertainty in the nuclear distribution is anticipated to become a limiting factor in extracting the precise value of the nuclear weak charge [44,45].

With the PNC matrix elements computed, now we compile the mixing coefficients $-i\eta_{nn}$, Eq. (10), see Table II. We use accurate energies of the $ns_{1/2}$ and $np_{1/2}$ states from Refs. [46–50]. We estimate radiative widths Γ by summing spontaneous emission rates [51] over all the possible $E1$ decay channels. The relevant atomic data are collected in Table III.

We find that all the tabulated PNC mixing coefficients are comparable, even though the PNC matrix elements scale as $1/n^3$. This is attributed to the decreasing energy splittings with increasing principal quantum number. It is worth reemphasizing that our calculations in this section assume the absence of magnetic fields; Zeeman level crossings are discussed in Sec. III.

The PNC amplitude for the $n's - ns$ transition [53] can be simplified to

$$E_{\rm PNC} = \overline{\langle ns_{1/2}m_j}|D_z|\overline{n's_{1/2}m_j\rangle}$$
$$= \frac{1}{3}\left[\sum_\mu \eta^*_{n\mu}(\mu p_{1/2}||r||n's) + \sum_\nu \eta_{n'\nu}(ns||r||\nu p_{1/2})\right], \tag{16}$$

where $(\mu p_{1/2}||r||n's)$ and $(ns||r||\nu p_{1/2})$ are the radial integrals of the electric dipole operator. Notice that the overall phase of the PNC amplitude is not fixed as it depends on the relative phases of the two $s_{1/2}$ states.

PNC amplitudes in hydrogen are dominated by the mixing between the near-degenerate energy levels. Then the $2s-3s$ and $2s-4s$ PNC amplitudes evaluate to

$$E_{\rm PNC}(2s-3s) = \tfrac{1}{3}[\eta^*_{33}(3p_{1/2}||r||2s) + \eta_{22}(3s||r||2p_{1/2})]$$
$$= 3.504i\times 10^{-13}\ \text{a.u.},$$
$$E_{\rm PNC}(2s-4s) = \tfrac{1}{3}[\eta^*_{44}(4p_{1/2}||r||2s) + \eta_{22}(4s||r||2p_{1/2})]$$
$$= 1.531i\times 10^{-13}\ \text{a.u.}, \tag{17}$$

where we use the FN-R mixing coefficients from Table II. In addition, the dipole matrix elements were obtained with the relativistic analytic wave functions. Note that the $2s-3s$ PNC amplitude is three times larger than the $2s-4s$ one, mainly because of its larger dipole matrix element. The latter is just a little smaller than that for the $1s-2s$ transition, i.e., $E_{\rm PNC}(1s-2s) = 1.897i\times 10^{-13}$ a.u..

III. POSSIBLE EXPERIMENTAL REALIZATION

We turn now to consider how this PNC moment might be measured in a laboratory. For this we suggest a two-color coherent-control process, as was demonstrated in Refs. [54,55]. Rasor and Yost [30] considered a similar scheme. This all-optical approach is similar in some regards to the microwave measurements of the Michigan [13–17], Yale [18–20], and Washington [21–23] hydrogen PNC experiments. To measure the $\langle 3p_{1/2}m_j|H_W|3s_{1/2}m_j\rangle$ matrix elements, we suggest generating a slow, high-density atomic hydrogen beam, exciting the ground-state atoms to the metastable $2s\,^2S_{1/2}$, α_0 state via two-photon excitation with 243.1-nm light, and driving the $2s\,^2S_{1/2}$, $\alpha_0 \rightarrow 3s\,^2S_{1/2}$, β_0 transition using three distinct interfering interactions

TABLE II. PNC mixing coefficients $-i\eta_{nn}$, Eq. (10), multiplied by a factor of 10^{13}. $\Delta E_n = E_{ns} - E_{np_{1/2}}$ is the energy splitting, and $\Delta\Gamma = \Gamma_{np_{1/2}} - \Gamma_{ns}$ is the effective energy width.

	ΔE_n (MHz)	$\Delta\Gamma$ (MHz)	PN-NR	FN-NR	PN-R	FN-R	Others
$2s$–$2p_{1/2}$	1057.847	99.709	4.408	4.408	4.412	4.410	4.3[a]; 3.6[b]
$3s$–$3p_{1/2}$	314.818	29.187	4.779	4.778	4.782	4.780	–
$4s$–$4p_{1/2}$	133.2	12.231	4.893	4.893	4.897	4.895	–

[a]Moskalev [52]; Lewis and Williams [14].
[b]Dunford *et al.* [13].

(α_0 and β_0 are two hyperfine components of the $ns\ ^2S_{1/2}$ state, using the notation introduced by Lamb and Retherford [56].) This transition is electric dipole ($E1$) forbidden, but is active through Stark mixing when a static electric field is applied, as well as through the weak-interaction mixing. The wavelength of the laser beam that is resonant with this transition is 656.5 nm. See Fig. 1(a) for a partial energy level diagram of hydrogen. The transition is also active as a two-photon transition, driven by a field at a wavelength of $\lambda = 1313$ nm. (The two-photon interaction can also be driven with two unequal-frequency beams, providing flexibility of the selection rules for the transition, but also introducing experimental challenges. We will consider only the simpler form for now.) When the three interactions are driven concurrently, the net transition rate scales as the square of the sum of the individual amplitudes

$$\mathcal{R} = |A_{2\gamma} + A_{St} + A_{\rm PNC}|^2, \tag{18}$$

where $A_{2\gamma}$, $A_{\rm St}$, and $A_{\rm PNC}$ are the amplitudes for the two-photon, Stark-induced, and PNC-induced interactions, respectively. In the coherent control technique, only modest electric fields are required, such that the maximum Stark amplitude $|A_{\rm St}|$ is less than $\sim 5 \times A_{\rm PNC}$, and since $A_{\rm PNC}$ is very weak, a two-photon amplitude that is much greater than $A_{\rm St}$ or $A_{\rm PNC}$ is easily achieved. In this limit,

$$\mathcal{R} \approx |A_{2\gamma}|^2 + A_{2\gamma}^*(A_{\rm St} + A_{\rm PNC}) + \text{c.c.}, \tag{19}$$

where we omitted the small $|A_{\rm St} + A_{\rm PNC}|^2$ term. In this expression, $|A_{2\gamma}|^2$ represents the two-photon absorption rate by itself, while the cross term arises from the interference between the weak amplitudes ($A_{\rm St}$ and $A_{\rm PNC}$) and the strong two-photon amplitude. Coherence between the 1313-nm field and the 656-nm field is assured when the second is generated from the first through a second-harmonic generation process, which is inherently coherent. We illustrate a layout of laser sources in Fig. 1(b). A laser beam of wavelength 243 nm, generated through two stages of frequency doubling of the output of a 972.54-nm high-power laser diode, can be used to excite the $F = 1$ (α_0) component of the metastable $2s\ ^2S_{1/2}$ state. A second laser source, of wavelength 1313 nm, can be used to excite the $2s\,^2S_{1/2} \rightarrow 3s\,^2S_{1/2}$ transition via two-photon absorption, or, after frequency doubling to generate a 656-nm beam, through a linear interaction. The $2s\,^2S_{1/2}$ state is long lived, so loss of population as the atoms travel from the preparation region to the region where they interact with the two-color field (656 nm plus 1313 nm) is minimal. Upon phase shifting the 1313-nm beam, the interference between the linear excitation and the two-photon excitation of the $3s^2S_{1/2}$ state can be modulated, and the amplitude of this modulation, normalized by the two-photon rate alone, is

$$2\left\{\frac{A_{\rm St} + A_{\rm PNC}}{A_{2\gamma}}\right\}. \tag{20}$$

Since the amplitudes $A_{\rm St}$ and $A_{\rm PNC}$ are 90° out of phase with one another, the amplitude of the interference term scales as

$$2\left\{\frac{\sqrt{|A_{\rm St}|^2 + |A_{\rm PNC}|^2}}{A_{2\gamma}}\right\} \tag{21}$$

and measurement of this amplitude as a function of the applied static electric field can be used to determine the ratio $A_{\rm PNC}/A_{\rm St}$.

By applying a magnetic field to the atoms in the interaction region, the energy levels of the $3s$ and $3p_{1/2}$ states, and similarly the $4s$ and $4p_{1/2}$ states, can be made to cross. We illustrate the level crossings of the $3s$ and $3p_{1/2}$ states in Fig. 1(c). By bringing the levels into degeneracy, the admixture of states caused by the weak interaction can be enhanced by a factor of $\Gamma/\Delta E$, where Γ is radiative width of the state, and ΔE is the energy splitting at zero magnetic field. This enhancement factor is ~ 21 for the $3s$–$3p_{1/2}$ and the $4s$–$4p_{1/2}$ manifolds, very similar to that of the $2s$–$2p_{1/2}$ states. Bringing levels into degeneracy also allows for selection of specific combinations of coupling constants. We evaluated the Zeeman mixing of states, and the weak force interaction elements, and find very similar results for the $3s$–$3p_{1/2}$ and $4s$–$4p_{1/2}$ level crossings as were previously reported in the $2s$–$2p_{1/2}$ system. We compile these in Table IV. In this table, we include the magnetic field and the dependence of the weak interaction term on the coupling constants $C_p^{(1)}$ and $C_p^{(2)}$, which we

TABLE III. Properties of the hydrogen atom used in our numerical evaluations. $\Delta E_{\rm Lamb}$ is the energy difference (Lamb shift) between the ns and $np_{1/2}$ states and Γ are radiative level widths at zero magnetic and electric fields.

State	$\Delta E_{\rm Lamb}$ (MHz)	Γ (MHz)
$2s_{1/2}$	1057.847	0
$3s_{1/2}$	314.82	1.0050
$4s_{1/2}$	133.2	0.70251
$2p_{1/2}$	–	99.709
$3p_{1/2}$	–	30.192
$4p_{1/2}$	–	12.934

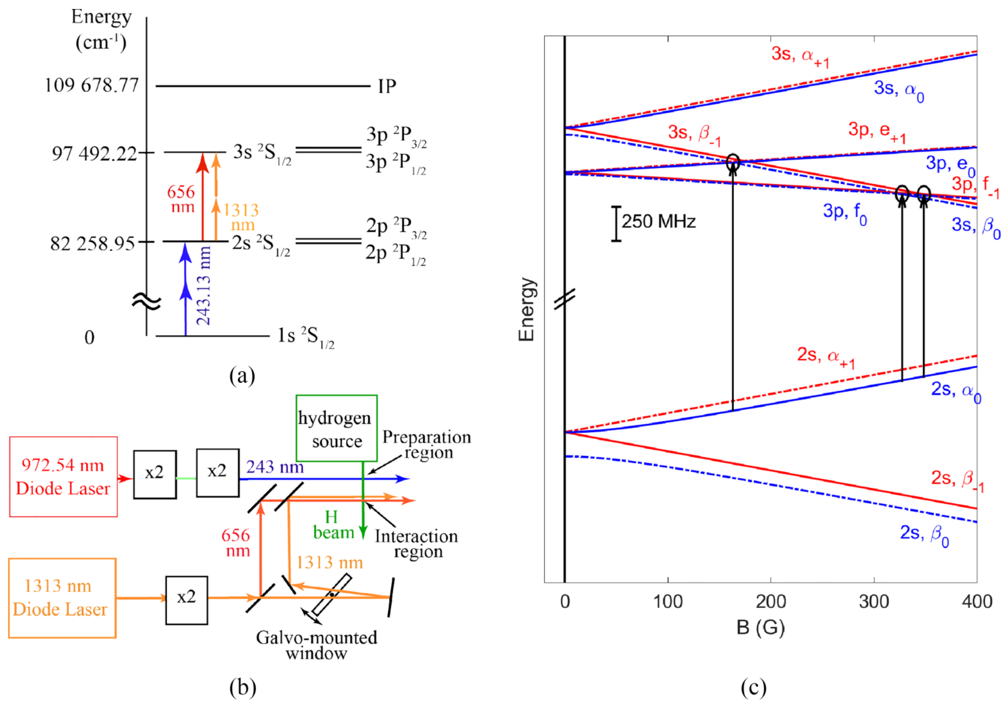

FIG. 1. (a) An energy level diagram showing the relevant levels of atomic hydrogen. (b) Experimental geometry for a coherent control measurement of $E_{\rm PNC}$ on the $2s\,^2S_{1/2} \rightarrow 3s\,^2S_{1/2}$ transition. (c) An energy level diagram showing the level crossings induced by the Zeeman shift. Three level crossings between the $3s\,^2S_{1/2}$ and $3p\,^2P_{1/2}$ are of interest in this work: $\beta_0 - e_0$ at $B = 163$ G, $\beta_0 - f_0$ at $B = 327$ G, and $\beta_{-1} - f_{-1}$ at $B = 348$ G. The optical transition from the $2s\,^2S_{1/2}, \alpha_0$ level will be driven by the two-color coherent laser field at 1313 nm and 656 nm simultaneously.

determine by evaluating the matrix elements of Eq. (8) [13]

$$\langle ns, m_J' m_I' | V_{\rm PV} | np_{1/2}, m_J m_I\rangle = +i\overline{V}\langle m_J' m_I' | \left[-C_p^{(1)} + 2C_p^{(2)} \boldsymbol{\sigma}\cdot\mathbf{I}\right] | m_J m_I\rangle. \quad (22)$$

(We omitted the third coupling constant $C_p^{(3)}$, which is expected to be much smaller than $C_p^{(2)}$ per the discussion in Sec. I.) In this expression, m_J and m_J' are the electronic and m_I and m_I' are the nuclear magnetic quantum numbers. $\boldsymbol{\sigma}$ is the Pauli spin operator for the electronic angular momentum, and $\mathbf{I}$ is the nuclear spin operator. The scaling factor $\overline{V} = (3G_{\rm F}/8\pi\sqrt{2})R_{n0}(0)R_{n1}'(0)(\hbar/m_e c)$ is as defined in Eq. (26) of Ref. [13], where $R_{n\ell}(0)$ is the radial nonrelativistic wave function at the origin and the prime denotes a derivative with respect to r. Evaluation of these terms with wave functions tabulated, e.g., in Ref. [40] leads to

$$\langle ns, m_J' m_I' | V_{\rm PV} | np_{1/2}, m_J m_I\rangle = +i\overline{V}\left\{\zeta_1 C_p^{(1)} + \zeta_2 C_p^{(2)}\right\}. \quad (23)$$

Since, in this section, we focus on the experimental feasibility, we use the approximation with a point-like nucleus and nonrelativistic electronic wave functions, which are sufficient for this goal, unless the experimental uncertainties reach the $<0.1\%$ level. We list the coefficients ζ_1 and ζ_2 for each level crossing in Table IV.The values of ζ_1 and ζ_2 for the $2s$–$2p_{1/2}$ level crossings are close to, but not quite the same as, those reported by Dunford, Lewis, and Williams [13]. Notice that the weak matrix element near the β_0–e_0 level crossing is relatively insensitive to the $C_p^{(1)}$ coupling constant for $n = 2$, 3, and 4, and this level crossing provides a hopeful avenue for a precision determination of $C_p^{(2)}$. In the absence of a magnetic field, a similar analysis leads to the matrix element

$$\langle ns\beta_0 | V_{\rm PV} | np_{1/2}\rangle = +i\overline{V}\left\{-C_p^{(1)} + C_p^{(2)}\right\}. \quad (24)$$

Systematic errors are known to play a critical role in PNC measurements, and careful attention to these effects is required to reduce their impact. Stray electric fields, which can strongly mix the $ns_{1/2}$ and np_j states, are expected to be more critical for $n = 3$ or 4 in the optical measurement than for

TABLE IV. The coefficients ζ_1 and ζ_2 of Eq. (23) yielding the relative contribution of $C_p^{(1)}$ and $C_p^{(2)}$ to $\langle ns, m_J' m_I' | V_{\rm PV} | np_{1/2}, m_J m_I\rangle$ at the different level crossings. Results for the different states $n = 2$, 3, and 4 are quite similar to one another. In the fourth column, we list the magnetic field of the level crossings.

Matrix element	ζ_1	ζ_2	B (G)
$2s$–$2p_{1/2}$			
$\langle\beta_0\|V_{\rm PV}\|e_0\rangle$	0.0002	−1.9858	552.14
$\langle\beta_0\|V_{\rm PV}\|f_0\rangle$	−0.9974	−0.8889	1157.39
$\langle\beta_{-1}\|V_{\rm PV}\|f_{-1}\rangle$	0.9970	−0.9970	1230.53
$3s$–$3p_{1/2}$			
$\langle\beta_0\|V_{\rm PV}\|e_0\rangle$	0.0006	−1.9854	164.39
$\langle\beta_0\|V_{\rm PV}\|f_0\rangle$	−0.9973	−0.8894	344.66
$\langle\beta_{-1}\|V_{\rm PV}\|f_{-1}\rangle$	0.9969	−0.9969	366.34
$4s$–$4p_{1/2}$			
$\langle\beta_0\|V_{\rm PV}\|e_0\rangle$	0.0013	−1.9846	69.48
$\langle\beta_0\|V_{\rm PV}\|f_0\rangle$	−0.9973	−0.8896	145.69
$\langle\beta_{-1}\|V_{\rm PV}\|f_{-1}\rangle$	0.9969	−0.9969	154.84

$n = 2$ in the rf measurements due to the larger electric dipole matrix elements $\langle ns_{1/2}||r||np_j\rangle$ for $n = 3$ or 4, and the smaller Lamb shift. However, the optical coherent control method eliminates the rf cavity and requires only modest static electric fields, allowing large spacing of the parallel field plates used to control the electric field. The larger distance between the hydrogen atoms and these conductors reduces the effect of surface contaminants and patch effects, which could introduce uncontrollable electric fields in the interaction region [57]. Still, control of the electric field is expected to be a challenge in this measurement. Using a perturbative analysis, we estimate that, for a dc electric field of magnitude $E_0 \sim 5\ \mu\text{V/cm}$, the Stark-induced amplitude A_{St} matches the PNC amplitude A_{PNC}. While this critical E_0 is $\sim$100 times greater than that for the $2s\ \beta_0 \to 3s\ \beta_0$ transition suggested in Ref. [30], achieving this level of control will require development of new laboratory techniques.

Reduction of systematic contributions to the PNC measurement, relative to the single-field rf measurement, are also expected from the method used for phase control. In the coherent control, optical measurement, shifting the laser field takes place external to the interaction region. In addition, the uniformity and tight control of linear polarization of laser beams, and the state selectivity of the two-photon interaction (that is, only transitions coupling the same initial and final states can interfere with the two-photon interaction) serve to further reduce systematic effects. Tight control of laser polarization also serves to reduce magnetic dipole ($M1$) contributions to the signal. While we are not aware of any calculations of the $M1$ amplitude for these transitions, it is expected to be small since the radial wave functions of the $2s$, $3s$, and $4s$ states are orthogonal to one another. If the relativistic effects are large enough to allow a weak $M1$ amplitude, this effect can be reduced by use of counterpropagating waves in a standing wave optical cavity. Use of standing wave field for this purpose, as well as for enhancement of the PNC amplitude, were used in Refs. [8,9]. Reduction of systematic effects for the general coherent control process are discussed in more detail in Ref. [55].

There are a couple of options available for detection of atoms that have transitioned to the $3s$ state. Note that, in addition to its sensitivity to $3s$ atoms, the detection method must be highly insensitive to atoms that are excited to the $3p_{1/2}$ state. The primary spontaneous decay paths for $3s$ atoms is to the $2p_{1/2}$ and $2p_{3/2}$ levels, followed by rapid decay to the $1s$ ground state. Detection of the Lyman alpha radiation of the $2p_j \to 1s$ line, therefore, seems a promising detection method for this measurement. Detection of the fluorescence at 656 nm from the first leg of this decay does not seem feasible, as it suffers from the likely copious presence of scattered laser light, and also from the spontaneous fluorescence resulting from the decay of $3p_{1/2}$ atoms to the $2s$ state, both of which would be at similar wavelengths, and therefore, difficult to separate. The $3p_{1/2}$ state can decay directly to the $1s$ ground state or to the $2s$ state. The 102.6-nm fluorescence due to the previous state must, therefore, be blocked, but the second state is not expected to interfere with the Lyman alpha detection, as the $2s$ state is long lived (lifetime $\sim$100 ms). A second detection option would be to apply a weak probe beam tuned to the $3s \to 2p_{3/2}$ line to the interaction region, and observe the gain in this probe beam. We choose this line as it is distinct from the interfering transitions used to populate the $3s$ level, in contrast to the detection method proposed in Ref. [30]. The frequency of this line differs from that of the excitation wavelength by $\sim$10 GHz. This probe laser intensity should be maintained at a level much less than the saturation intensity of the transition so as to not affect the $3s$ state population significantly. We note that the frequency of the 656-nm excitation beam is sufficient to photoionize the $3s$ state through a one-photon interaction. A detection scheme based on photoionization, however, is not feasible, as photoions generated from the $3p_{1/2}$ state would mask the $3s$ signal. In fact, this photoionization rate should be minimized to the extent possible to avoid space-charge effects that might otherwise obscure the signal.

Two-pathway coherent control allows for the measurement of very weak transition moments such as E_{PNC}, referenced against the Stark transition polarizability. The limiting systematic effect encountered in the previous microwave approach resulting from the mechanical rotation of a microwave cavity would not contribute to this optical measurement. As shown in this section, this all-optical approach can provide a precise measurement of $C_p^{(1)}$ and $C_p^{(2)}$. Given that these constants can be extracted simultaneously, we remind the reader that the axial charge g_A, determined by the $C_p^{(2)}/C_p^{(1)}$ ratio, is an important quantity in understanding the spin structure of the nucleon, and it also plays a role in certain astrophysical processes. It can be measured in the β decay of the neutron. Its currently recommended value [12] is $g_A = 1.2756(13)$. This value can provide a consistency check for the $C_p^{(2)}/C_p^{(1)}$ ratio.

IV. CONCLUSION

A long-standing goal in atomic parity violation has been a measurement in hydrogen. The attraction of hydrogen is two-fold. First, the electronic structure of hydrogen is much better known than that of any other atom, greatly facilitating interpretation of the results. Second, since the hydrogen nucleus contains only a single proton, measurement of the nuclear spin-independent coupling coefficient $C_p^{(1)}$ leads directly to $\sin^2\theta_{\text{W}}$. Prior measurements based on microwave transitions between hyperfine components of the $2s_{1/2}$ state were ultimately not successful. In the present work, we outlined how similar measurements carried out on the $2s_{1/2} \to 3s_{1/2}$ or $2s_{1/2} \to 4s_{1/2}$ transition might prove fruitful, and described an experimental technique for such an investigation.

ACKNOWLEDGMENTS

We are happy to acknowledge a useful discussion with R. Dunford. This work was supported by the U.S. National Science Foundation under Grants No. PHY-1912519 and No. PHY-2207546, and by the Sara Louise Hartman endowed professorship in physics. J.L. is grateful to the University of Nevada, Reno for its hospitality and acknowledges the financial support by the National Natural Science Foundation of China (Grant No. 11874090).

[1] M. S. Safronova, D. Budker, D. DeMille, D. F. J. Kimball, A. Derevianko, and C. W. Clark, Search for new physics with atoms and molecules, Rev. Mod. Phys. **90**, 025008 (2018).
[2] C. Wieman and A. Derevianko, Atomic parity violation and the standard model, arXiv:1904.00281.
[3] W. J. Marciano, Radiative corrections to neutral current processes, in *Precision Tests of the Standard Electroweak Model*, edited by P. Langacker (World Scientific, Singapore, 1995), p. 170.
[4] J. D. Bjorken and S. D. Drell, *Relativistic Quantum Mechanics* (McGraw-Hill, New York, 1964).
[5] W. J. Marciano and A. I. Sanda, Parity violation in atoms induced by radiative corrections, Phys. Rev. D **17**, 3055 (1978).
[6] J. Erler, A. Kurylov, and M. J. Ramsey-Musolf, Weak charge of the proton and new physics, Phys. Rev. D **68**, 016006 (2003).
[7] D. Androić, D. S. Armstrong, A. Asaturyan, T. Averett, J. Balewski, K. Bartlett, J. Beaufait, R. S. Beminiwattha, J. Benesch, F. Benmokhtar *et al.*, Precision measurement of the weak charge of the proton, Nature (London) **557**, 207 (2018).
[8] C. S. Wood, S. C. Bennett, D. Cho, B. P. Masterson, J. L. Roberts, C. E. Tanner, and C. E. Wieman, Measurement of parity nonconservation and an anapole moment in cesium, Science **275**, 1759 (1997).
[9] D. Antypas, A. Fabricant, J. E. Stalnaker, K. Tsigutkin, V. V. Flambaum, and D. Budker, Isotopic variation of parity violation in atomic ytterbium, Nat. Phys. **15**, 120 (2019).
[10] T. Aaltonen, S. Amerio, D. Amidei, A. Anastassov, A. Annovi, J. Antos, G. Apollinari, J. A. Appel, T. Arisawa, A. Artikov *et al.* (CDF Collaboration), High-precision measurement of the W boson mass with the CDF II detector, Science **376**, 170 (2022).
[11] H. B. Tran Tan and A. Derevianko, Implications of W-Boson mass anomaly for atomic parity violation, Atoms **10**, 149 (2022).
[12] R. L. Workman, V. D. Burkert, V. Crede, E. Klempt, U. Thoma, L. Tiator, K. Agashe, G. Aielli, B. C. Allanach, C. Amsler *et al.* (Particle Data Group), Review of particle physics, Prog. Theor. Exp. Phys. **2022**, 083C01 (2022).
[13] R. W. Dunford, R. R. Lewis, and W. L. Williams, Parity nonconservation in the hydrogen atom. II, Phys. Rev. A **18**, 2421 (1978).
[14] R. R. Lewis and W. L. Williams, Parity nonconservation in the hydrogen atom, Phys. Lett. B **59**, 70 (1975).
[15] R. W. Dunford, Parity violating neutral current interactions and $2S_{12} \to 2S'_{12}$ transitions in hydrogenic ions, Phys. Lett. B **99**, 58 (1981).
[16] L. P. Lévy and W. L. Williams, Role of damping and T Invariance in induced transition in H(2S), Phys. Rev. Lett. **48**, 1011 (1982).
[17] C. C. W. Fehrenbach, An experimental limit on parity mixing in atomic hydrogen, Ph.D. thesis, University of Michigan, 1993.
[18] E. Hinds and V. Hughes, Parity nonconservation in hydrogen involving magnetic/electric resonance, Phys. Lett. B **67**, 487 (1977).
[19] E. Hinds, Sensitivity and the role of level crossings in measurements of parity nonconservation using metastable atoms, Phys. Rev. Lett. **44**, 374 (1980).
[20] E. Hinds and V. Hughes, Parity nonconservation in hydrogen involving magnetic/electric resonance, in *A Festschrift In Honor Of Vernon W Hughes* (World Scientific, Singapore, 1992), pp. 178–179.
[21] E. Adelberger, T. Trainor, E. Fortson, T. Chupp, D. Holmgren, M. Iqbal, and H. Swanson, A technique for measuring parity non-conservation in hydrogenic atomis, Nucl. Instrum. Methods **179**, 181 (1981).
[22] E. N. Fortson and L. Lewis, Atomic parity nonconservation experiments, Phys. Rep. **113**, 289 (1984).
[23] P. W. Wong, *The Search for Parity Nonconservation in Hydrogen* (University of Washington, Seattle, 1990).
[24] M. Bouchiat and C. Bouchiat, I. Parity violation induced by weak neutral currents in atomic physics, J. Phys. **35**, 899 (1974).
[25] M. Bouchiat and C. Bouchiat, Parity violation induced by weak neutral currents in atomic physics. part II, J. Phys. **36**, 493 (1975).
[26] R. Dunford, PNC in hydrogen. Different prospects using heliumlike ions, Technical Report ANL/PHY/CP-97343 (Argonne National Laboratory, Argonne, IL, 1998).
[27] R. W. Dunford and R. J. Holt, Parity violation in hydrogen revisited, J. Phys. G: Nucl. Part. Phys. **34**, 2099 (2007).
[28] R. W. Dunford and R. J. Holt, Parity nonconservation in hydrogen, Hyperfine Interact. **200**, 45 (2011).
[29] M. DeKieviet, T. Gasenzer, O. Nachtmann, and M.-I. Trappe, Longitudinal atomic beam spin echo experiments: a possible way to study parity violation in hydrogen, Hyperfine Interact. **200**, 35 (2011).
[30] C. Rasor and D. C. Yost, Laser-based measurement of parity violation in hydrogen, Phys. Rev. A **102**, 032801 (2020).
[31] N. Koch and E. Steffens, High intensity source for cold atomic hydrogen and deuterium beams, Rev. Sci. Instrum. **70**, 1631 (1999).
[32] A. Huber, B. Gross, M. Weitz, and T. W. Hänsch, High-resolution spectroscopy of the 1S-2S transition in atomic hydrogen, Phys. Rev. A **59**, 1844 (1999).
[33] D. Szczerba, L. van Buuren, J. van den Brand, H. Bulten, M. Ferro-Luzzi, S. Klous, H. Kolster, J. Lang, F. Mul, H. Poolman *et al.*, A polarized hydrogen/deuterium atomic beam source for internal target experiments, Nucl. Instrum. Methods Phys. Res., Sect. A **455**, 769 (2000).
[34] N. Kolachevsky, M. Fischer, S. G. Karshenboim, and T. W. Hänsch, High-precision optical measurement of the 2S hyperfine interval in atomic hydrogen, Phys. Rev. Lett. **92**, 033003 (2004).
[35] S. D. Hogan, A. W. Wiederkehr, M. Andrist, H. Schmutz, and F. Merkt, Slow beams of atomic hydrogen by multistage zeeman deceleration, J. Phys. B: At., Mol. Opt. Phys. **41**, 081005 (2008).
[36] M. Mikirtychyants, R. Engels, K. Grigoryev, H. Kleines, P. Kravtsov, S. Lorenz, M. Nekipelov, V. Nelyubin, F. Rathmann, J. Sarkadi *et al.*, The polarized H and D atomic beam source for ANKE at COSY-Jülich, Nucl. Instrum. Methods Phys. Res., Sect. A **721**, 83 (2013).
[37] S. F. Cooper, Z. Burkley, A. D. Brandt, C. Rasor, and D. C. Yost, Cavity-enhanced deep ultraviolet laser for two-photon cooling of atomic hydrogen, Opt. Lett. **43**, 1375 (2018).
[38] W. R. Johnson, *Atomic Structure Theory: Lectures on Atomic Physics* (Springer-Verlag, Berlin, 2007).
[39] W. Greiner, *Relativistic Quantum Mechanics*, 3rd ed. (Springer-Verlag, Berlin, 2000).

[40] *Springer Handbook of Atomic, Molecular, and Optical Physics*, 2nd ed., edited by G. W. F. Drake (Springer, New York, 2005).

[41] G. Feinberg and M. Chen, $2S_{1/2} \to 1S_{1/2}+$ one-photon decay of muonic atoms and parity-violating neutral-current interactions, Phys. Rev. D **10**, 190 (1974).

[42] G. W. F. Drake, Theory of transitions, and the electroweak interaction, in *The Spectrum of Atomic Hydrogen: Advances*, edited by G. Series (World Scientific, Singapore, 1988), Chap. 3, pp. 137–241.

[43] I. B. Khriplovich, *Parity Nonconservation in Atomic Phenomena* (Gordon and Breach, Philadelphia, 1991), p. 319.

[44] B. A. Brown, A. Derevianko, and V. V. Flambaum, Calculations of the neutron skin and its effect in atomic parity violation, Phys. Rev. C **79**, 035501 (2009).

[45] A. Derevianko, Correlated many-body treatment of the Breit interaction with application to cesium atomic properties and parity violation, Phys. Rev. A **65**, 012106 (2001).

[46] A. Kramida, A critical compilation of experimental data on spectral lines and energy levels of hydrogen, deuterium, and tritium, At. Data Nucl. Data Tables **96**, 586 (2010).

[47] M. Horbatsch and E. A. Hessels, Tabulation of the bound-state energies of atomic hydrogen, Phys. Rev. A **93**, 022513 (2016).

[48] N. Bezginov, T. Valdez, M. Horbatsch, A. Marsman, A. C. Vutha, and E. A. Hessels, A measurement of the atomic hydrogen Lamb shift and the proton charge radius, Science **365**, 1007 (2019).

[49] C. W. Fabjan, F. M. Pipkin, and M. Silverman, Radiofrequency spectroscopy of hydrogen fine structure in $n = 3, 4, 5$, Phys. Rev. Lett. **26**, 347 (1971).

[50] H. Fleurbaey, S. Galtier, S. Thomas, M. Bonnaud, L. Julien, F. Biraben, F. Nez, M. Abgrall, and J. Guéna, New measurement of the $1S-3S$ transition frequency of hydrogen: contribution to the proton charge radius puzzle, Phys. Rev. Lett. **120**, 183001 (2018).

[51] A. Kramida, Y. Ralchenko, J. Reader, and NIST ASD TEAM, NIST Atomic Spectra Database (version 5.7) [Online] (2019), doi: 10.18434/T4W30F.

[52] A. Moskalev, Weak neutral currents in atoms and μ-mesic atoms, JEPT Lett. **19**, 141 (1974).

[53] S. G. Porsev, K. Beloy, and A. Derevianko, Precision determination of electroweak coupling from atomic parity violation and implications for particle physics, Phys. Rev. Lett. **102**, 181601 (2009).

[54] D. Antypas and D. S. Elliott, Measurement of a weak transition moment using two-pathway coherent control, Phys. Rev. A **87**, 042505 (2013).

[55] D. Antypas and D. Elliott, Measurement of weak optical transition moments through two-pathway coherent control, Can. J. Chem. **92**, 144 (2014).

[56] W. E. Lamb, Jr. and R. C. Retherford, Fine structure of the hydrogen atom. Part I, Phys. Rev. **79**, 549 (1950).

[57] C. Speake, Forces and force gradients due to patch fields and contact-potential differences, Class. Quantum Grav. **13**, A291 (1996).